

Self-Balancing of Cell Populations via Martingale Turnover with Amplification

Authors

Tomoyuki Yamaguchi*

Affiliations

Research Institute, Nozaki Tokushukai Hospital,
2-10-50 Tanigawa, Daito City, Osaka, 574-0074 Japan
Tel: +81-72-874-1641, Fax: +81-72-818-3723

*Corresponding author: t.yamaguchi@tokushukai.jp

Key words: Stochastic simulation; Population dynamics; Random walk; Immune regulation; Unified theory; Entropy

Abstract

The mechanisms underlying adaptive control in biological systems, such as intestinal immune regulation, remain poorly understood, despite detailed knowledge of their regulatory networks. Here, we propose an alternative to traditional deterministic regulation. We theoretically demonstrate that stochastic martingale turnover—in which cells proliferate through mutual competition and decay without component-specific control—naturally converges to an appropriate population balance characterized by a low probability of cell loss. This compositional change is described by a modified Langevin equation, where conserved mass is replaced by a dynamic variable representing the fitness of the current composition. A random walk model with step lengths that shorten near the target, together with its mathematical solution, demonstrates entropy increase under favorable conditions. Thus, we propose a fundamental principle for autonomous biological control.

Introduction

Living systems exhibit remarkable adaptability under diverse and fluctuating conditions. While molecular biology has uncovered many genetically predetermined causal relationships among genes and cells, the mechanisms that enable adaptive control—especially in the presence of biological noise—remain unclear (1-3). For example, in intestinal immunity, effector T lymphocytes (Teff) are essential for preventing bacterial enterocolitis, whereas regulatory T lymphocytes (Treg) suppress excessive immune responses to prevent inflammatory bowel disease (4). A key challenge has been to elucidate the mechanisms that maintain an appropriate balance between Teff and Treg populations. Recently, ROR γ t-expressing antigen-presenting cells (ROR γ t⁺ APCs) were identified as key activators of Treg, playing a critical role in maintaining this balance (5-9). However, additional mechanisms are required to explain how the system balances ROR γ t⁺ APCs and Teff-activators (4, 10). The endless complexity of these regulatory networks implies that the enormous accumulation of finely defined parameters may still be insufficient to fully explain the dynamic adaptability of biological systems.

Inspired by recent advances in artificial intelligence, particularly reinforcement learning algorithms in AlphaGo and DeepSeek-R1 (11, 12), we hypothesize that a trial-and-error process for optimizing outcomes may be embedded in biological systems (13-15). In previous work, we proposed that gene expression regulation through epigenetic modifications constitutes a form of self-optimization (16). In that model, epigenetic states, such as histone acetylation levels, were assumed to change stochastically through amplification, noise, and decay, at equal probabilities across a pair of gene loci, while the decay rates are affected by the expression ratio of the two genes. Stochastic simulations demonstrated that gene expression ratios autonomously stabilize as decay rates decline (16). Here, we apply this gene regulation model to the autonomous balance of two cell populations. By formalizing this process as a stochastic differential equation similar to the Langevin equation, we reveal how biological adaptability naturally emerges.

Stochastic turnover with amplification for balanced coexistence

First, we investigate how two cell populations, such as Teff and Treg in intestinal immunity, can balance autonomously in stochastic simulations of an abstract model. To this end, we extend our previous model of gene expression regulation (16) to describe the population dynamics of two cell types, I and II. We define the number of cells of type i at time t as $N_i(t)$, where $i \in \{I, II\}$, and $N_i(t)$ is a non-negative integer. As in traditional birth-death models, cell numbers change through stochastic processes of increase and decrease (Fig. 1A). The increase consists of two processes: intrinsic proliferation and extrinsic influx. To be noticed, in the proliferation and decay processes, each cell has an equal probability of dividing or dying, regardless of cell type, but these probabilities vary over time, in our model.

For increase due to proliferation, the probability that the number of cells of type i increases by one in the infinitesimal time interval $[t, t+dt]$ is given by:

$$P(N_i(t+dt) = N_i(t) + 1 | N(t)) = a \frac{N_i(t)}{\sum_j N_j(t)} dt \quad (1),$$

where $N(t) = (N_I(t), N_{II}(t))$. This equation represents competitive amplification in proliferation; one cell is randomly selected for dividing into two cells, and all cells compete equally for shared proliferation resources regardless of cell type (Fig. 1A-B). This is similar to Pólya's urn, where one ball in a urn is randomly drawn and a ball with the same color is added together with the drawn ball (17). The ratio of colored balls in the urn is a martingale; a stochastic process where the expected value of the next observation is equal to the present value. Notably, a bounded martingale converges almost surely (18), which may be important for autonomous balancing.

For influx due to migration or differentiation, the probability that the cell number increases by one is given by:

$$P(N_i(t+dt) = N_i(t) + 1 | N(t)) = b_i dt \quad (2),$$

which represents a biased influx with a specific probability to cell-type i (Fig. 1C).

For decay, each cell is removed with a decay probability $\lambda(N(t))dt$ in the time interval $[t, t+dt]$. The number of removed cells follows a binomial distribution:

$$P(N_i(t+dt) = n | N(t)) = \frac{N_i(t)!}{n! (N_i(t) - n)!} (1 - \lambda(N(t))dt)^n (\lambda(N(t))dt)^{N_i(t) - n} \quad (3),$$

where $n \in \{0, 1, \dots, N_i(t)\}$. We assume that the appropriateness of the ratio $N_I(t) : N_{II}(t)$ enhances cell survival. Thus, $\lambda(N(t))$ is typically an increasing function of the deviation of the present population ratio $X(t) \equiv N_I(t)/\sum N_j(t)$ from the target α .

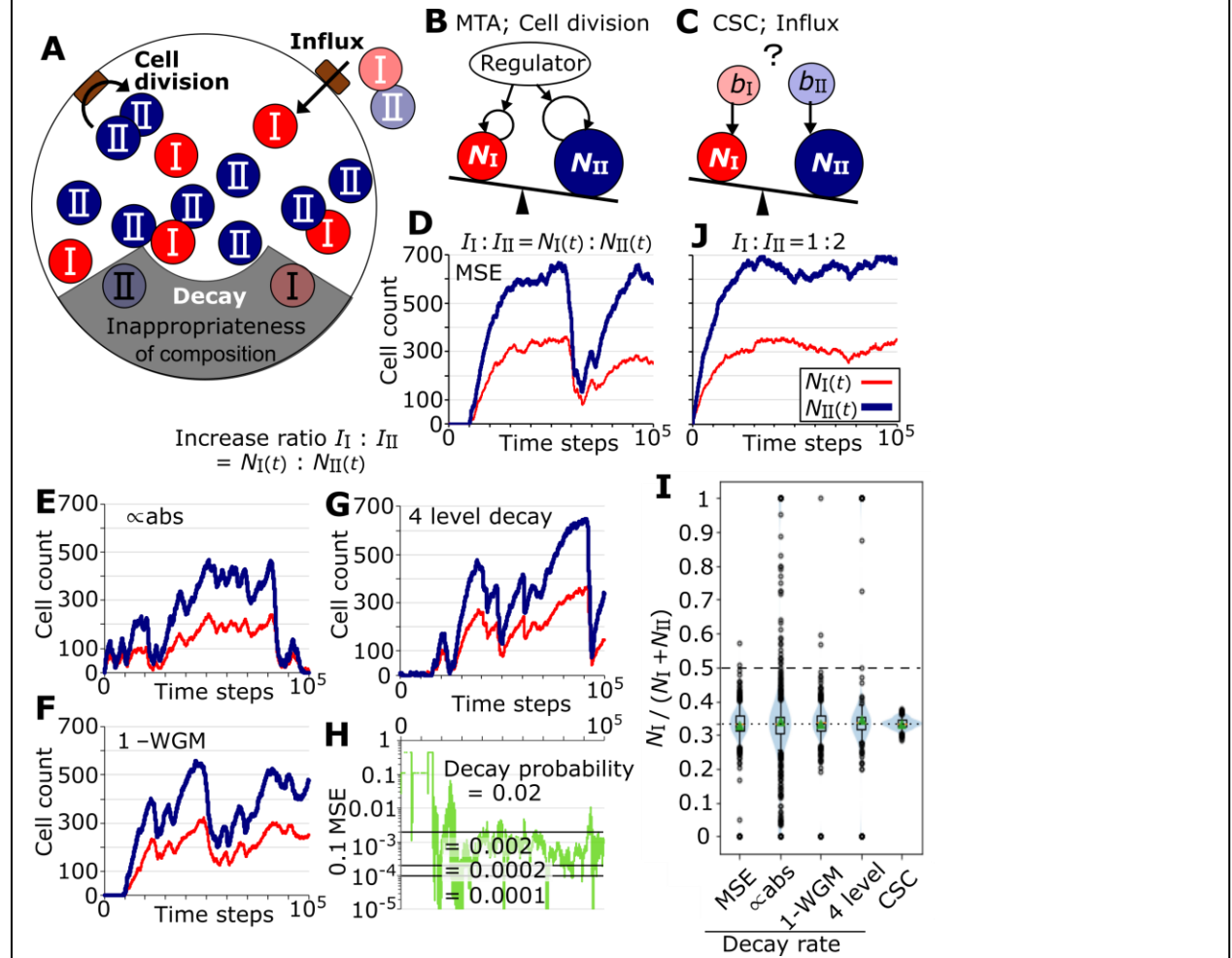


Fig. 1. Adaptive and predetermined controls for balancing two cell populations. (A-C) Cell numbers $N_I(t)$ and $N_{II}(t)$ change through three stochastic processes; increase by competitive proliferation at a $N_I(t) : N_{II}(t)$ ratio, increase by influx at a fixed $b_I : b_{II}$ ratio, and decrease with a decay rate depending on the composition. **(B)** In Martingale Turnover with Amplification (MTA), each individual cell has an equal probability, regardless of cell type. **(C)** In Component-Specific Control (CSC), the predetermined influx ratio must be controlled by extrinsic factors. **(D-G, J)** Cell numbers $N_I(t)$ and $N_{II}(t)$ are plotted over time in representative simulations. **(D)** In MTA with “MSE”, decay rate is $0.1(N_I/\sum N_j(t) - 1/3)^2$. **(E)** In MTA with “ $\propto \text{abs}$ ”, decay rate depends on the absolute difference, $|N_I/\sum N_j(t) - 1/3|/60$. **(F)** In MTA with “1-WGM”, weighted geometric mean is used for decay rate. **(G, H)** In MTA with “4 level”, four discrete probabilities based on MSE are used as shown in (H). **(I)** Violin plots with box-whisker plots for $N_I/\sum N_j(t)$ at $t=10^5$ from 1,000 simulations, excluding $\sum N_j(t) = 0$. Triangle marks indicate the mean. The initial and target values are 1/2 and 1/3, respectively. **(J)** In CSC, the increase ratio $I_I : I_{II}$ is fixed at 1 : 2.

To evaluate whether these stochastic processes can regulate population ratio, we performed stochastic simulations with time step $dt = 1$. Under a condition favoring intrinsic proliferation ($a \gg b_i$, specifically $a = 0.1$ and $b_i = 0.0005$), the population ratio ($X(t)$, $1 - X(t)$) autonomously approached the target (α , $1 - \alpha$), when the decay probability was set to k times the mean squared error (MSE), $\lambda(N(t)) = k(X(t) - \alpha)^2$, with $k, \alpha = 0.1, 1/3$ (Fig. 1D) (16). To be noticed, the competition, which is represented by $1/\sum N_j(t)$ in Eq. (1), and a small but non-zero influx b_i in Eq. (2) prevent divergence, extinction, or monopolization by a single cell type (16). We also examined alternative decay functions; absolute difference (Fig. 1E), $1 - \exp$ of the Kullback-Leibler divergence, which is equivalent to the weighted geometric mean (WGM) of present composition to target (Fig. 1F), and 4 levels of stepwise decay probability based on MSE (Fig. 1G-H). All these decay functions effectively maintained the population ratio near the target for most time points (Fig. 1, D-H) and across most simulations at $t = 10^5$ (Fig. 1I).

The framework encompasses a distinct regime of deterministic control; cell numbers increase exclusively via influx by setting the proliferation probability $a = 0$. For example, with $a = 0$, $\lambda(X(t)) = 10^{-4}$, $b_I = 0.033$, and $b_{II} = 0.067$, the ratio $N_I(t) : N_{II}(t)$ correctly approached the target ratio $1 : 2$, without initial lag or occasional fluctuations (Fig. 1J), with a small variance at $t = 10^5$ (Fig. 1I). However, this process is not adaptive, as it requires prior specification of the influx ratio $b_I : b_{II}$.

In summary, two distinct mechanisms can achieve a convergence of composition $N_I(t) : N_{II}(t) \cong \alpha : (1 - \alpha)$, with its optimal cell-increase ratio $I_I : I_{II} \cong \alpha : (1 - \alpha)$. One is Component-Specific Control (CSC), which relies on predetermined proper influx ratio $I_I : I_{II} = b_I : b_{II} = \alpha : (1 - \alpha)$. The other is Martingale Turnover with Amplification (MTA), which sets the increase ratio $I_I : I_{II} = N_I(t) : N_{II}(t)$ and dynamically adjusts a common decay probability for all cells. While CSC deterministically increases cells via influx under extrinsic control, MTA increases cells via intrinsic amplification with giving each cell an equal opportunity without altering the expected population-ratio at the next time point (Fig. 1A-C).

Mathematical description of stochastic simulations of population balance

Next, we mathematically formalize the regulation processes in MTA and CSC. By taking an infinitesimal time interval dt , we can assume that the probability for two or more cells to increase or decrease in dt is negligible compared to the probability of a single event (19). When the number of cells of type i , $N_i(t)$, changes according to Eqs. (1-3), the expectation (denoted by $\langle \cdot \rangle$) of the change of $N_i(t)$ over dt becomes:

$$\frac{\langle dN_i(t) \rangle}{dt} = a \frac{N_i(t)}{\sum_j N_j(t)} - \lambda(N(t)) N_i(t) + b_i \quad (4).$$

This equation is nearly identical to those previously introduced in models for gene expression regulation (16) and immune regulation (20).

Since the amplification parameter a and decay rate $\lambda(N(t))$ are consistent across all cell types at each time point, summing Eq. (4) over both cell types gives the expected change in the total cell number $M(t) \equiv \sum_j N_j(t)$:

$$\frac{\langle dM(t) \rangle}{dt} = a - \lambda(X(t)) M(t) + b \quad (5),$$

where $b \equiv \sum b_j$, and decay rate is expressed as $\lambda(X(t))$ since this is determined by composition $X(t) \equiv N_I(t)/M(t)$. Notably, Eq. (5) is equivalent to the equation describing stochastic degradation turnover in general biological systems (21). In other words, our model distinguishes between the intrinsic amplification of components and the extrinsic component-specific influx, in the construction process of stochastic degradation turnover.

Given that $0 < \lambda(X(t)) < 1$, Eq. (5) shows that the expectation of the total population size converges to:

$$\langle M(t) \rangle \cong \frac{a + b}{\lambda(X(t))} \quad (6).$$

Since the MTA and CSC processes regulate cell composition $X(t)$, we focus on the change to $X(t)$ in dt . In the increase processes of cells, $X(t)$ increases with probability $(aX(t) + b_I)dt$ by an amount $(1 - X(t))/(M(t) + 1)$, and decreases with probability $(a(1 - X(t)) + b_{II})dt$ by $X(t)/(M(t) + 1)$. In the decay process of cells, $X(t)$ increases with probability $\lambda(X(t))M(t)(1 - X(t))dt$ by $X(t)/(M(t) - 1)$, and decreases with probability $\lambda(X(t))M(t)X(t)dt$ by $(1 - X(t))/(M(t) - 1)$. These changes give the expectation and the variance $V(\cdot)$ of the composition change:

$$\frac{\langle dX(t) \rangle}{dt} = \frac{b}{M(t) + 1} (\beta - X(t)) \quad (7)$$

$$\frac{V(dX(t))}{dt} = X(t)(1 - X(t)) \left(\frac{a}{(M(t) + 1)^2} + \frac{\lambda(X(t))M(t)}{(M(t) - 1)^2} \right) + \frac{b(X^2(t) - 2\beta X(t) + \beta)}{(M(t) + 1)^2} \quad (8),$$

where $\beta \equiv b_I/b$. Equation (7) demonstrates that the stochastic process of $X(t)$ in MTA with $b = 0$ is a martingale; $\langle X(t + dt) \rangle = X(t)$. Under conditions $\lambda(X(t))M(t) \cong a + b$ and $M(t) \gg 1$, the variance simplifies to:

$$\frac{V(dX(t))}{dt} \cong \frac{\sigma^2(X(t))}{M^2(t)} \quad (9)$$

$$\sigma^2(X(t)) \equiv 2aX(t)(1 - X(t)) + b(X(t) - 2\beta X(t) + \beta) \quad (10).$$

Since $X(t)$ is in range $[0, 1]$, the variance is highly dependent on $M(t)$ when $X(t)$ is not near the boundaries, particularly $X(t) \cong \alpha$. Then, we can approximate the variance using a constant parameter σ :

$$\frac{V(dX(t))}{dt} \cong \frac{\sigma^2}{M^2(t)} \quad (11)$$

$$\sigma \equiv \sqrt{2a\alpha(1 - \alpha) + b(\alpha + \beta - 2\alpha\beta)} \quad (12).$$

These approximations are valid under conditions where both cell populations are sufficiently abundant and the composition remains close to the target; $M(t) \gg 1$, $X(t) \cong \alpha$, and $\lambda(X(t))M(t) \cong a + b$. Therefore, situations involving catastrophic deterioration or small population size should be excluded from the following analysis.

Then, the stochastic differential equation (SDE) describing composition change is given by:

$$\frac{dX(t)}{dt} = \frac{b}{M(t)} (\beta - X(t)) + \frac{\sigma\eta(t)}{M(t)} \quad (13),$$

where $\eta(t)$ is temporally uncorrelated Gaussian white noise. Alternatively, substituting Eq. (6) for $M(t)$ gives:

$$\frac{dX(t)}{dt} = \frac{b}{a + b} \lambda(X(t)) \left(\beta + \frac{\sigma\eta(t)}{b} - X(t) \right) \quad (14).$$

This formulation reveals that decay rate $\lambda(X(t))$, and intrinsic and extrinsic increase parameters a and b , dynamically shape the evolution of composition. Multiplying both sides of Eq. (13) by $M(X(t))dt$, we obtain:

$$M(X(t))dX(t) = b(\beta - X(t))dt + \sigma dW(t) \quad (15),$$

where $W(t)$ is a Wiener process (Brownian motion). The Wiener process is the integral of white noise $\eta(t)$ and is normally distributed with mean 0 and variance t . The first term on the right-hand side represents a drift with kinetic friction. Remarkably, Eq. (15) is analogous to the Langevin equation, which describes the stochastic dynamics of a particle under kinetic friction and biased random force. In contrast to physical systems where mass is conserved, in our non-equilibrium open biological systems with turnover, the “mass” $M(X(t))$ —representing resistance to change—is a dynamic quantity dependent on composition fitness. Thus, we propose Eq. (15) as a unified formulation of biological and physical phenomena, highlighting the fundamental role of “dynamic resistance to change” in autonomous biological systems.

Stability analysis of critical points in MTA and CSC

The mathematical formulation clarifies the asymptotic behavior of $X(t)$ and the role of stochastic noise in MTA. When the decay function $\lambda(X(t))$ is modeled as MSE, i.e., $\lambda(X(t)) = (\alpha - X(t))^2$, Eq. (14) becomes:

$$\frac{dX(t)}{dt} = \frac{b}{a+b} \left(\beta + \frac{\sigma\eta(t)}{b} - X(t) \right) (\alpha - X(t))^2 \quad (16).$$

Tentatively fixing the noise value, we can plot $dX(t)/dt$ as a function of $X(t) = x$ (Fig. 2).

In the CSC regime, the large influx parameter $b \gg a$ makes the noise term $\sigma\eta(t)/b$ small. Under this condition, $\beta + \sigma\eta(t)/b$ is like a fixed point where $X(t)$ becomes stable. Another candidate α is a saddle point. Specifically, if $\alpha < \beta$, then $X(t) < \alpha$ increases toward α , slowing as it approaches α (blue curve in Fig. 2). However, once $X(t) > \alpha$, $X(t)$ moves rapidly away from α toward $\beta + \sigma\eta(t)/b$ with acceleration. Conversely, if $\alpha > \beta$, then $X(t) > \alpha$ decreases toward $\beta + \sigma\eta(t)/b$ with transient slowing down near α (red curve in Fig. 2). Thus, in CSC, $X(t)$ tends to stabilize around β with limited fluctuation.

In contrast, under the MTA regime where $b \cong 0$, the noise term $\sigma\eta(t)/b$ becomes large—its magnitude exceeds both β and $X(t)$. As a result, the putative fixed point $\beta + \sigma\eta(t)/b$ in CSC becomes unstable due to the large noise. The sign of $dX(t)/dt$ fluctuates depending on the instantaneous sign of $\eta(t)$, causing frequent reversal in increase and decrease of $X(t)$ (e.g., switching blue and red curves in Fig. 2). Therefore, $X(t)$ behaves as a type of random walk that decreases step lengths near α . Because of critical slowing down around the saddle point at α and frequent stochastic reversals of movement direction, $X(t)$ tends to stay near α for extended periods, consistent with simulation results (Fig. 1D) and mathematical analysis in the next section. Interestingly, whereas CSC suppresses noise effects to stabilize $X(t)$ near β , MTA relies on noise-driven fluctuations to control $X(t)$ near α .

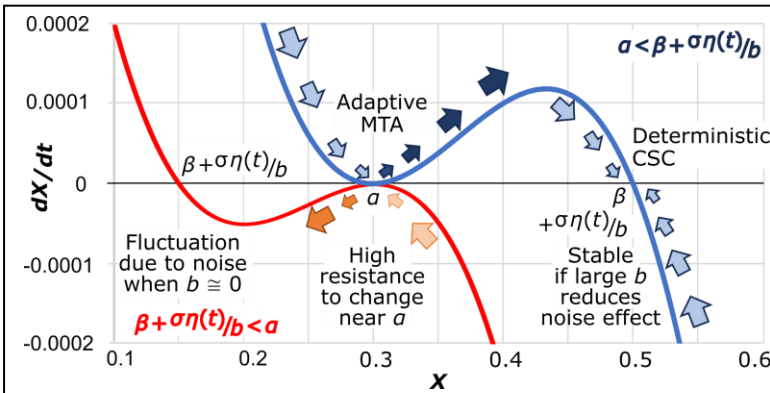


Fig. 2. Stability of critical points in adaptive MTA and deterministic CSC. The change rate $dX(t)/dt$ is plotted against $X(t)$ under two conditions; $b/(a+b)=0.1$, $\alpha=0.3$, $\beta=0.5$, and $\sigma\eta(t)/b=0$ (blue), or $\beta + \sigma\eta(t)/b=0.15$ (red), in Eq. (16). The fixed point at $\beta + \sigma\eta(t)/b$ is stable only when noise is restricted by a sufficiently large b . The saddle point α has both stable and unstable neighbors on each curve.

Random walk controlling the step length

We will solve the SDE under simplified conditions and elucidate the stochastic dynamics of cell populations in Fig. 1. In the absence of a deterministic drift term (i.e., $b = 0$ in Eqs. (14-15)), the behavior of $X(t)$ under MTA becomes a random walk in which the step length varies depending on the present position. Substituting $b = 0$ into Eq. (15) gives:

$$dY_t = \frac{1}{M(Y_t)} dW_t \quad (17),$$

where $Y_t = |X(t/\sigma^2) - \alpha|$ denotes the distance to target value α . Note that W_t is a Wiener process that is characterized by $dt = (dW_t)^2$. To solve Eq. (17) for the decay functions used in Fig. 1, we consider the equivalent formulation:

$$dY_t = \frac{\lambda(Y_t)}{a} dW_t \quad (18),$$

which is derived from Eq. (14) under the condition $b = 0$.

In a random walk relevant to Fig. 1E, the decay rate increases linearly with the distance to target; $\lambda(Y_t) = akY_t$ with $0 < k < 1$. Substituting into Eq. (18) gives:

$$dY_t = kY_t dW_t$$

and the solution: $Y_t = Y_0 \exp\left(-\frac{k^2}{2}t + kW_t\right)$ (19),

where Y_0 is the initial distance to the target. This is a geometric Brownian motion without a drift term, a model widely used in mathematical finance (22). In this random walk, even with a 50% chance of moving in the correct direction, smaller steps in better (closer) positions and larger steps in worse (farther) positions yields a $(1 - k^2)$ -fold improvement in positioning after two steps

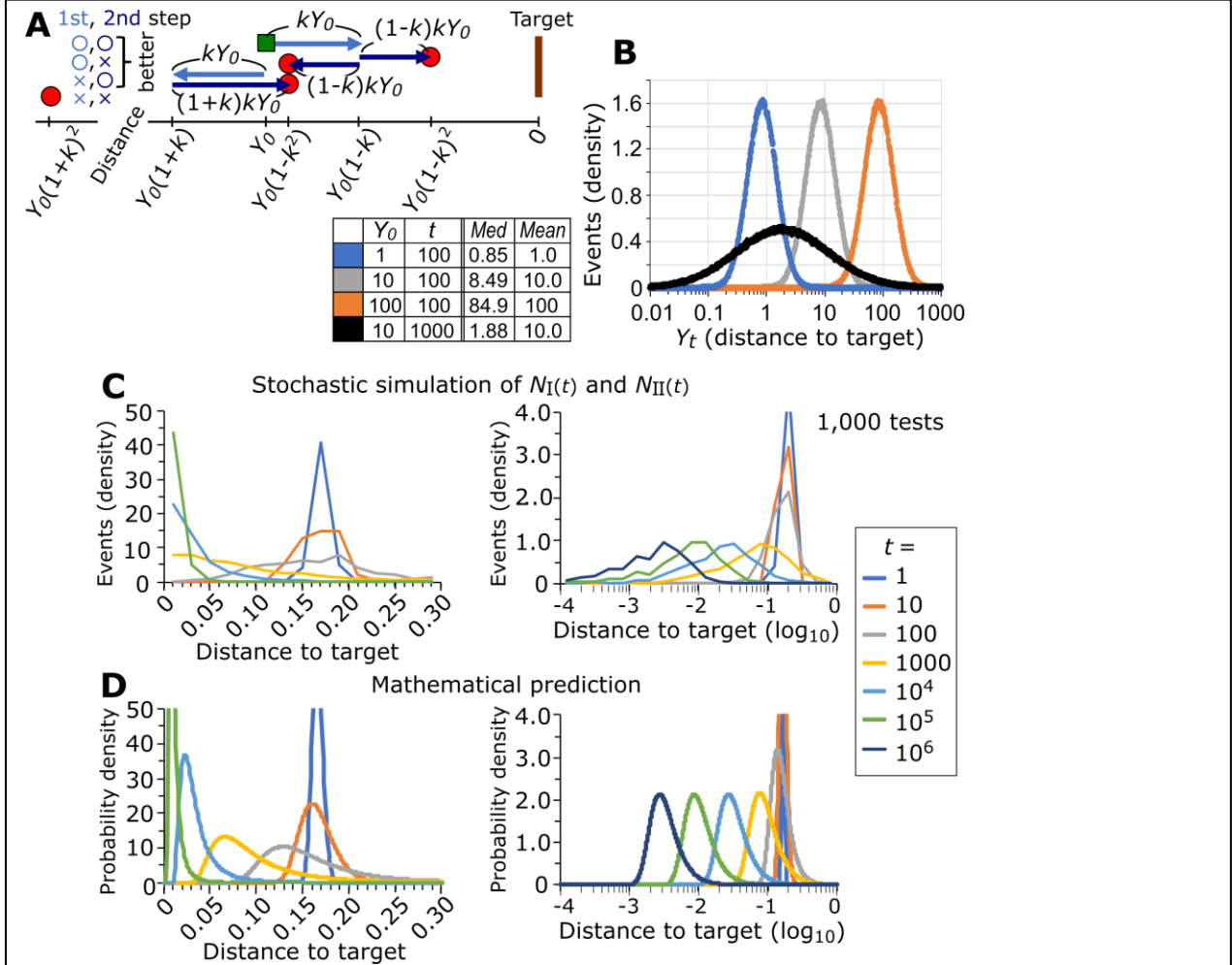


Fig. 3. Step-length controlling random walk as an MTA process. (A) The agent moves from the initial position Y_0 (green square) to new positions (red circles) by repeating steps in random directions with step length proportional to the current distance, kY_t . Correct and incorrect step directions are indicated by \circ and \times , respectively. **(B)** In random walk simulations with a maximum step length of $0.1Y_t$, the agent's positions after 100 and 1,000 steps are shown as histogram on a logarithmic scale. Y_0 : initial distance; *Med*: median. **(C)** In 1,000 stochastic simulations, two cell populations change the numbers $N_I(t)$ and $N_{II}(t)$ by competitive amplification (with probability $a = 0.1$) and decay (with probability 0.1MSE) without any additive increase. The distance to the target, $|N_I/\Sigma N_j(t) - 1/3|$, is shown as histogram at indicated time points (from $t = 1$ to 10^5 and 10^6) on linear and logarithmic scales. **(D)** Probability density functions are calculated from Eq. (22) setting $k = 1$, $\sigma^2 = 4/90$, $Y_0 = 1/6$, and shown on linear and logarithmic scales.

in half of the cases (Fig. 3A). We verify this behavior through stochastic simulations, where Y_{t+1} is randomly selected from a uniform distribution in range $[0.9Y_t, 1.1Y_t]$ (Fig. 3B). Consistent with Eqs. (18-19) using $k^2 = 1/300$, the distance Y_t follows log-normal distributions with a constant mean but a progressively decreasing median over time. Thus, even without directional control, agents autonomously approach the target through repeated steps in most cases.

In a model relevant to Fig. 1D, the decay rate is based on MSE; $\lambda(Y_t) = akY_t^2$. Substituting into Eq. (18) gives:

$$dY_t = kY_t^2 dW_t \quad (20).$$

Applying Itô's formula with the transformation $Z_t = 1/(kY_t)$, we obtain:

$$dZ_t = \frac{k^2 Y_t^4}{2} \frac{\partial^2 Z_t}{\partial y^2} dt + kY_t^2 \frac{\partial Z_t}{\partial y} dW_t = kY_t dt - dW_t = \frac{1}{Z_t} dt - dW_t \quad (21).$$

This is the SDE of a three-dimensional Bessel process, where Z_t represents the radial component of three-dimensional Brownian motion (23). As $t \rightarrow \infty$, it is known that $Z_t \rightarrow \infty$ almost surely, implying $Y_t \rightarrow 0$. The corresponding probability density function of Y_t is:

$$p(y, t|Y_0) = \frac{Y_0}{\sigma k \sqrt{2\pi t} y^3} \left(\exp\left(-\frac{1}{2\sigma^2 k^2 t} \left(\frac{1}{y} - \frac{1}{Y_0}\right)^2\right) - \exp\left(-\frac{1}{2\sigma^2 k^2 t} \left(\frac{1}{y} + \frac{1}{Y_0}\right)^2\right) \right) \quad (22).$$

To confirm the accuracy of mathematical analysis, we compared the theoretical prediction with stochastic simulations of two-population dynamics governed by Eqs. (1) and (3). In this simulation, the cell numbers $N_I(t)$ and $N_{II}(t)$ undergo competitive amplification (with $a = 0.1$) and decay based on MSE, $\lambda(X(t)) = 0.1(X(t) - \alpha)^2$ with target $\alpha = 1/3$. The initial condition was set to $N_I(0) = N_{II}(0) = 18$. To avoid extinction, cell number $N_i(t)$ was reset to one if it drew zero in decay process. Using Eq. (12), we estimate the noise intensity $\sigma^2 = 2a\alpha(1 - \alpha) \cong 0.044$. Figure 3C shows the evolution of the distance $|X(t) - \alpha|$ in 1,000 stochastic simulations, while Fig. 3D displays the theoretical distribution of the distance predicted by Eq. (22). Although the simulations had larger variance than the prediction, the medians similarly converged to zero over time without changing the distribution broadness on a logarithmic scale. Thus, Eq. (22) describes population dynamics in MSE model under MTA condition.

Autonomous balancing in biological systems

As the probability density function in Eq. (22) becomes a Dirac delta function at $y = 0$ as $t \rightarrow \infty$, the law of increasing entropy provides a natural explanation for the autonomous control inherent to the MTA process. We define entropy as the number of possible microstates—not the degree of disorder. When a microstate $N(t)$ yields a composition $N_I/\sum N_j(t)$ close to a particular value, the number of microstates increases as the total cell number $\sum N_j(t)$ grows. Notably, inappropriate compositions rarely permit large total cell numbers. Therefore, the number of accessible microstates becomes large near appropriate states, even though such biologically ordered states may appear far from disordered. Supporting this view, biological systems are characterized by high individual-level diversity—a striking contrast to the uniformity of artificial machines.

The regulation of intestinal immunity illustrates how MTA theory offers new insights into biological control. In the conventional CSC framework, when $\text{ROR}\gamma^+$ APCs activate Treg as key regulators (4-9), they are assumed not to activate Teff. In contrast, although the cellular relevance in the actual immune system remains to be clarified, the MTA framework proposes that a key regulator reduces the decay probability of both Treg and Teff populations. Supporting this view, $\text{ROR}\gamma^+$ cells are essential for the formation of secondary lymphoid organs (24), enhance the survival of both Treg and Teff populations (25), and are more abundant in healthy intestines than in inflammatory conditions (6). Thus, theoretically, the Treg/Teff ratio would converge to a balance in which $\text{ROR}\gamma^+$ APCs—characteristic of a healthy intestine—are prevalent. MTA theory suggests that a healthy intestine could be both a consequence and a cause of balanced immunity, naturally arising from the large number of microstates, or high entropy, near the optimal balance.

Our MTA theory indicates that biological “appropriateness”—typically synonymous with low-decay, stable conditions—emerges autonomously through stochastic turnover involving replication and degradation. In contrast, conventional molecular and systems biology often underappreciate such self-optimizing processes due to their inherent stochasticity and causal ambiguity (13, 14). Most biologists—including authors and reviewers—tend to favor the CSC framework, in which key regulators exert specific, reproducible effects on particular cell types. In this view, high specificity is equated with biological importance, while non-specific, martingale-type effects are often overlooked or remain unpublished. This bias may contribute to the reproducibility crisis in biological research. Reinterpreting biological data through the lens of MTA could reveal underlying mechanisms of autonomous optimization and reduce reliance on elusive extrinsic factors.

References

1. P. Meyer, J. Saez-Rodriguez, Advances in systems biology modeling: 10 years of crowdsourcing DREAM challenges. *Cell Syst* **12**, 636-653 (2021). doi:10.1016/j.cels.2021.05.015
2. Z. R. Thornburg *et al.*, Fundamental behaviors emerge from simulations of a living minimal cell. *Cell* **185**, 345-360 e328 (2022). doi:10.1016/j.cell.2021.12.025
3. N. Eling, M. D. Morgan, J. C. Marioni, Challenges in measuring and understanding biological noise. *Nature Reviews Genetics* **20**, 536-548 (2019). doi:10.1038/s41576-019-0130-6
4. R. Kedmi, D. R. Littman, Antigen-presenting cells as specialized drivers of intestinal T cell functions. *Immunity* **57**, 2269-2279 (2024). doi:10.1016/j.immuni.2024.09.011
5. B. Akagbosu *et al.*, Novel antigen-presenting cell imparts T(reg)-dependent tolerance to gut microbiota. *Nature* **610**, 752-760 (2022). doi:10.1038/s41586-022-05309-5
6. M. Lyu *et al.*, ILC3s select microbiota-specific regulatory T cells to establish tolerance in the gut. *Nature* **610**, 744-751 (2022). doi:10.1038/s41586-022-05141-x
7. R. Kedmi *et al.*, A ROR γ ⁺ cell instructs gut microbiota-specific T_{reg} cell differentiation. *Nature* **610**, 737-743 (2022). doi:10.1038/s41586-022-05089-y
8. P. F. Rodrigues *et al.*, Ror γ -positive dendritic cells are required for the induction of peripheral regulatory T cells in response to oral antigens. *Cell* **188**, 2720-2737.e2722 (2025). doi:10.1016/j.cell.2025.03.020
9. L. Fu *et al.*, Prdm16-dependent antigen-presenting cells induce tolerance to gut antigens. *Nature*, (2025). doi:10.1038/s41586-025-08982-4
10. M. C. Campos Canesso *et al.*, Identification of antigen-presenting cell–T cell interactions driving immune responses to food. *Science* **387**, eado5088 (2025). doi:10.1126/science.ado5088
11. D. Silver *et al.*, Mastering the game of Go with deep neural networks and tree search. *Nature* **529**, 484-489 (2016). doi:10.1038/nature16961
12. DeepSeek-AI *et al.*, DeepSeek-R1: Incentivizing Reasoning Capability in LLMs via Reinforcement Learning. *arXiv*, 2501.12948 (2025). doi:10.48550/arXiv.2501.12948
13. G. Pezzulo, M. Levin, Top-down models in biology: explanation and control of complex living systems above the molecular level. *J R Soc Interface* **13**, (2016). doi:10.1098/rsif.2016.0555
14. E. O. Neftci, B. B. Averbeck, Reinforcement learning in artificial and biological systems. *Nature Machine Intelligence* **1**, 133-143 (2019). doi:10.1038/s42256-019-0025-4
15. V. Vanchurin, Y. I. Wolf, M. I. Katsnelson, E. V. Koonin, Toward a theory of evolution as multilevel learning. *Proc Natl Acad Sci U S A* **119**, (2022). doi:10.1073/pnas.2120037119
16. T. Yamaguchi, Learning processes in hierarchical pairs regulate entire gene expression in cells. *Sci Rep* **12**, 7549 (2022). doi:10.1038/s41598-022-10998-z

17. K. B. Athreya, S. Karlin, Embedding of Urn Schemes into Continuous Time Markov Branching Processes and Related Limit Theorems. *The Annals of Mathematical Statistics* **39**, 1801-1817 (1968).
18. J. L. Doob, *Stochastic Processes*. (Wiley, 1953).
19. D. T. Gillespie, The chemical Langevin equation. *The Journal of Chemical Physics* **113**, 297-306 (2000). doi:10.1063/1.481811
20. T. Yamaguchi *et al.*, Theoretical modeling reveals that regulatory T cells increase T-cell interaction with antigen-presenting cells for stable immune tolerance. *Int Immunol* **31**, 743-753 (2019). doi:10.1093/intimm/dxz043
21. P. W. Reddien, The purpose and ubiquity of turnover. *Cell* **187**, 2657-2681 (2024). doi:10.1016/j.cell.2024.04.034
22. F. Black, M. Scholes, The Pricing of Options and Corporate Liabilities. *Journal of Political Economy* **81**, 637-654 (1973).
23. M. Katori, in *Bessel Processes, Schramm–Loewner Evolution, and the Dyson Model*. (Springer Singapore, Singapore, 2016), pp. 1-39.
24. G. Eberl *et al.*, An essential function for the nuclear receptor RORgamma(t) in the generation of fetal lymphoid tissue inducer cells. *Nat Immunol* **5**, 64-73 (2004). doi:10.1038/ni1022
25. A. Jarade, J. P. Di Santo, N. Serafini, Group 3 innate lymphoid cells mediate host defense against attaching and effacing pathogens. *Curr Opin Microbiol* **63**, 83-91 (2021). doi:10.1016/j.mib.2021.06.005

Acknowledgments

I wish to thank Tetsuya. J. Kobayashi, Yumiko Imai, Masashi Kawaichi, and Yasuhiro Yamaguchi for their review and helpful suggestion on this research. We used AI tools (DeepSeek-r1 and ChatGPT-4o) to assist in the mathematical analysis, and ChatGPT-4o and DeepL Write as language aids to improve clarity and style.

Funding: This work was financially supported by the Tokushukai Medical Group.

Author contributions: T.Y. performed conceptualization, investigation, and writing.

Competing interests: Authors declare that they have no competing interests.

Data and materials availability: All data are available in the main text or the supporting information. The Python-based source code used for simulation and analysis is available at <https://github.com/tyamaguc-tky/Martingale>.

Materials and Methods

We performed Monte Carlo simulations using Python-based source codes, available at <https://github.com/tyamaguc-tky/Martingale>.

Stochastic simulation of the change of two cell populations

In the model describing the dynamics of the numbers of two cell types, I and II, under MTA and CSC conditions (Fig. 1), the stochastic processes of increasing and decreasing the cell numbers $N_I(t)$ and $N_{II}(t)$ were repeated $t = 10^5$ time steps. Initial values were set to $N_I(0) = N_{II}(0) = 1$ in Fig. 1 and $N_I(0) = N_{II}(0) = 18$ in Fig. 3C. The target ratio for $N_I(t) : N_{II}(t)$ was set to $\alpha : (1 - \alpha) = 1/3 : 2/3$.

In the MTA models (Fig. 1D-H), competitive proliferation occurs with probability $a = 0.1$ at each time step. When this intrinsic amplification proceeds, either cell type I or II is selected at the present ratio of $N_I(t) : N_{II}(t)$, and the chosen cell type increases the number (either $N_I(t)$ or $N_{II}(t)$) by one, if $N_I(t) + N_{II}(t) > 0$. If $N_I(t) + N_{II}(t) = 0$, proliferation does not occur. As for influx (migration and differentiation), additive increase occurs with probability $b_{\text{add}} = 0.001$. When this extrinsic increase proceeds, either cell type I or II is selected at a fixed probability $b_I : b_{II}$, and the selected cell type increases its number by one. In the MTA regime, $b_I : b_{II} = 1 : 1$. In decrease

process, each cell is removed at probability $\lambda(N(t))$ at each time step. The number $N_i(t+1)$ after decay is determined stochastically using a binomial distribution with $N_i(t)$ trials and success probability $1 - \lambda(N(t))$. The same $\lambda(N(t))$ is applied to both cell types. The decay probability $\lambda(N(t))$ is a function of the difference between the current cell ratio $X(t) = N_I(t)/(N_I(t) + N_{II}(t))$ and its target $\alpha = 1/3$, as described below. The minimum value of $\lambda(N(t))$ is set to 10^{-4} in Fig. 1.

- MSE model (Fig. 1D):

The decay probability is set to k times the mean squared error (MSE). Specifically, $\lambda(N(t)) = k \text{MSE}_{X(t)} = 0.1(X(t) - \alpha)^2$ if $(X(t) - \alpha)^2 > 10^{-3}$. If $(X(t) - \alpha)^2 \leq 10^{-3}$, $\lambda(N(t)) = 10^{-4}$. The initial decay probability $\lambda(N(0)) = 0.1(1/2 - 1/3)^2 = 1/360$. In the following models, parameter k is adjusted with setting the initial decay value $\lambda(N(0))$ to $1/360$.

- α abs model (Fig. 1E):

The decay probability is set to k times the absolute difference. Specifically, $\lambda(N(t)) = k |X(t) - \alpha|$, with $k = 1/60$ if $|X(t) - \alpha|/60 > 10^{-4}$. If $|X(t) - \alpha|/60 \leq 10^{-4}$, $\lambda(N(t)) = 10^{-4}$.

- 1 - WGM model (Fig. 1F):

The Kullback-Leibler divergence D_{KL} of the current composition $P = (X(t), 1 - X(t))$ from the target composition $Q = (\alpha, 1 - \alpha)$ is used for the decay function. The KL divergence is a type of statistical distance defined as $D_{KL}(P||Q) = \sum P(j) \log(P(j)/Q(j))$. The survival probability through a decay process at each time step is modeled as:

$$\begin{aligned} \exp(-k D_{KL}(P||Q)) &= \exp\left(-k \sum_j P_j \ln\left(\frac{P_j}{Q_j}\right)\right) = \prod_j \left(\frac{Q_j}{P_j}\right)^{k P_j} \\ &= \left(\frac{\alpha}{X(t)}\right)^{k X(t)} \left(\frac{1-\alpha}{1-X(t)}\right)^{k(1-X(t))} = \left[\left(\frac{\alpha}{X(t)}\right)^{X(t)} \left(\frac{1-\alpha}{1-X(t)}\right)^{1-X(t)}\right]^k = \text{WGM}^k \quad (\text{S1}), \end{aligned}$$

where WGM stands for the Weighted Geometric Mean of the relative appropriateness across all cell types. It lies in range $[0, 1]$, with yielding 1 when $X(t) = \alpha$. Thus, the decay probability at each time step is set: $\lambda(N(t)) = 1 - \text{WGM}^k = 1 -$

$\left(\frac{\alpha}{X(t)}\right)^{k X(t)} \left(\frac{1-\alpha}{1-X(t)}\right)^{k(1-X(t))}$ if $1 - \text{WGM}^k > 10^{-4}$. If $1 - \text{WGM}^k \leq 10^{-4}$, $\lambda(N(t)) = 10^{-4}$. For consistency with the MSE model, k is set such that: $\lambda(N(0)) = 1 - (2/3)^{k/2} (4/3)^{k/2} = 1 - (8/9)^{k/2} = 1/360$. Solving gives $k = 2 \log(1 - 1/360) / \log(8/9) \cong 0.0472$.

Notably, when the state $X(t)$ is transformed to the difference to the target $Y(t) \equiv \alpha - X(t)$, a condition $Y(t) \cong 0$ gives the following approximation:

$$\begin{aligned} \lambda(N(t)) &= 1 - \text{WGM}^k = 1 - \left(\frac{\alpha}{X(t)}\right)^{k X(t)} \left(\frac{1-\alpha}{1-X(t)}\right)^{k(1-X(t))} \\ &= 1 - \left(\frac{\alpha}{\alpha - Y(t)}\right)^{k(\alpha - Y(t))} \left(\frac{1-\alpha}{1-\alpha + Y(t)}\right)^{k(1-\alpha + Y(t))} \\ &= 1 - \left(1 + \frac{Y(t)}{\alpha - Y(t)}\right)^{k(\alpha - Y(t))} \left(1 - \frac{Y(t)}{1-\alpha + Y(t)}\right)^{k(1-\alpha + Y(t))} \\ &\cong 1 - (1 + kY(t))(1 - kY(t)) = (kY(t))^2 = k^2(\alpha - X(t))^2 \quad (\text{S2}). \end{aligned}$$

This approximation explains the comparable results in simulations using MSE and 1 - WGM models, as shown in Fig. 1I.

- In 4 level decay model (Fig. 1G-H):

The decay probability is assigned to four levels of stepwise values based on 0.1 times MSE, selected from $\{10^{-4}, 0.0002, 0.002, 0.02\}$. Specifically, $\lambda(N(t)) = 10^{-4}$ if $(X(t) - \alpha)^2 \leq 10^{-3}$, $\lambda(N(t)) = 0.0002$ if $10^{-3} < (X(t) - \alpha)^2 \leq 0.002$, $\lambda(N(t)) = 0.002$ if $0.002 < (X(t) - \alpha)^2 \leq 0.02$, and $\lambda(N(t)) = 0.02$ if $0.02 < (X(t) - \alpha)^2$.

In CSC model (Fig. 1J), cells do not proliferate via amplification (i.e., $a = 0$). Instead, cells increase only through influx, which occurs with probability $b_{add} = 0.1$ at each time step. When this extrinsic influx proceeds, either cell type I or II is selected at $b_I : b_{II} = \alpha : (1 - \alpha) = 1/3 : 2/3$ and the selected cell type increases the number by one. For decay, both $N_I(t)$ and $N_{II}(t)$ decrease with a fixed probability $\lambda(N(t)) = 10^{-4}$, using a binomial distribution.

In Fig. 1I, to plot $X(t) = N_I(t)/(N_I(t) + N_{II}(t))$, we excluded data with $N_I(t) + N_{II}(t) = 0$ at $t = 10^5$. From 1,000 simulations, we analyzed 997, 999, 993, 968, and 1,000 data with $N_I(t) + N_{II}(t) \neq 0$ in MSE, α abs, 1 –WGM, 4 level decay, and CSC models, respectively.

Stochastic simulation and its mathematical relevance

For the simulation in Fig. 3C, the cell numbers of type I and II, $N_I(t)$ and $N_{II}(t)$, change according to the MSE model with slight modification under the MTA conditions. Specifically, the decay probability at each time step, $\lambda(N(t)) = k \text{MSE}_{X(t)} = 0.1(X(t) - \alpha)^2$ if $(X(t) - \alpha)^2 > 10^{-7}$. If $(X(t) - \alpha)^2 \leq 10^{-7}$, $\lambda(N(t)) = 10^{-8}$, where $X(t) = N_I(t)/(N_I(t) + N_{II}(t))$ and its target $\alpha = 1/3$. Competitive amplification (increase by one after selected at the $N_I(t) : N_{II}(t)$ ratio) occurs with a probability $a = 0.1$ at each time step. The extrinsic influx probability b_{add} is set to 0. However, to prevent extinction, when $N_i(t) = 0$ after decay process, the $N_i(t)$ is reassigned to 1. The initial cell numbers are set to $N_I(0) = N_{II}(0) = 18$, because the initial cell ratio $X(0) = 1/2$ and $aX(0)/\lambda(X(0)) = 1/2 / (1/2 - 1/3)^2 = 18$. Starting from the initial distance $|X(0) - \alpha| = |1/2 - 1/3| = 1/6$, the distance to the target $|X(t) - \alpha|$ is recorded at time points $10^0, 10^1, 10^2, \dots, 10^6$ across 1,000 simulations. Histograms on a linear scale (bin width 0.02) display the density as event counts/1000/0.02. The results at time point 10^6 are excluded from the linear scale plot because they overlap the y-axis. Histograms on a logarithmic scale (bin width 0.2) display density as event counts/1000/0.2.

To compare with the simulation results, probability densities are calculated by using Eq. (22) with parameters $k = 1$, $\sigma^2 = 4/90$, $Y_0 = 1/6$ for Fig. 3D. As for the estimation of σ^2 , we use Eq. (12) with $a = 0.1$, $b = 0$, $\alpha = 1/3$. Therefore, $\sigma^2 = 2a\alpha(1 - \alpha) = 4/90 \cong 0.44$. On a logarithmic scale, we plot $f(x) = (\ln 10)10^x p(10^x, t)$.

Step-length controlling random walk

We performed stochastic simulations of a one-dimensional random walk in which the step length decreases as the agent approaches the target. The target is set to the origin, and the initial distance (position) Y_0 is set to 1, 10, or 100. At each time step, a random value d_{rand} is chosen from a uniform distribution in range $[-1, 1]$. From position Y_t , the agent moves to a new position $Y_{t+1} = Y_t + 0.1Y_t d_{rand}$, resulting in Y_{t+1} being drawn from a uniform distribution in range $[0.9Y_t, 1.1Y_t]$. We collected Y_t data after 100 and 1,000 steps over 10^6 simulations. Histograms on a logarithmic scale show the distributions of Y_t with its bin width $w = 0.005$. The plotted density is calculated as event counts/ $10^6 w = 0.0002$ counts.

The variance of a uniform distribution in range $[0.9Y_t, 1.1Y_t]$ is $V = (1.1Y_t - 0.9Y_t)^2/12 = 0.04Y_t^2/12 = Y_t^2/300$. Therefore, the diffusion coefficient $k^2 = 1/300$ in Eq. (19). Substituting this value into the expression for the median position $Q_{1/2}[Y_t] = Y_0 \exp(-k^2 t/2)$, we obtain $Q_{1/2}[Y_{100}] = 0.846Y_0$ and $Q_{1/2}[Y_{1000}] = 0.189Y_0$. These theoretical calculations are consistent with the simulation results shown in Fig. 3B.

Statistical Analysis

No statistical methods were used to predetermine the sample size in stochastic simulations. The investigators were not blinded to allocation during simulations and outcome assessment.

Supplementary Text

Mathematical Analysis

Here, we explain the derivation of equations in the text.

Equation (4):
$$\frac{\langle dN_i(t) \rangle}{dt} = a \frac{N_i(t)}{\sum_j N_j(t)} - \lambda(N(t)) N_i(t) + b_i$$

By taking a time interval dt so small, three stochastic reactions described by Eqs. (1-3) occurs mutually exclusively. The expectation (denoted by $\langle \cdot \rangle$) of the change of $N_i(t)$ over dt becomes Eq. (4). Further, we obtain the variance (denoted by $V(\cdot)$) of the change of cell number:

$$\begin{aligned} V(dN_i(t)) &= \frac{a N_i(t) dt}{\sum_j N_j(t)} \left(1 - \frac{a N_i(t) dt}{\sum_j N_j(t)} \right) + \lambda(N(t)) dt (1 - \lambda(N(t)) dt) N_i(t) + b_i dt (1 - b_i dt) \\ &\cong \left[a \frac{N_i(t)}{\sum_j N_j(t)} + \lambda(N(t)) N_i(t) + b_i \right] dt \end{aligned} \quad (S3).$$

Therefore, we obtain the SDE of the cell number:

$$\frac{dN_i(t)}{dt} = a \frac{N_i(t)}{\sum_j N_j(t)} - \lambda(N(t)) N_i(t) + b_i + \sigma_i(N(t)) \eta(t) \quad (S4),$$

where $\sigma_i(N(t)) \equiv \sqrt{a \frac{N_i(t)}{\sum_j N_j(t)} + \lambda(N(t)) N_i(t) + b_i}$ and $\eta(t)$ is temporally uncorrelated Gaussian white noise.

Equation (5):
$$\frac{\langle dM(t) \rangle}{dt} = a - \lambda(X(t)) M(t) + b$$

By taking a time interval dt so small, at most one cell increases or decreases during an infinitesimal time interval $[t, t+dt]$. Then, summing Eq. (4) over all cell types gives the expected change in the total cell number $M(t) \equiv \sum_j N_j(t)$ as Eq. (5). Further, we obtain the variance of the change of total cell number:

$$\begin{aligned} V(dM(t)) &= a dt (1 - a dt) + \lambda(X(t)) dt (1 - \lambda(X(t)) dt) M(t) + b dt (1 - b dt) \\ &\cong [a + \lambda(X(t)) M(t) + b] dt \end{aligned} \quad (S5).$$

Therefore, we obtain the SDE of the total cell number:

$$\frac{dM(t)}{dt} = a - \lambda(N(t)) M(t) + b + \sigma_M(N(t)) \eta(t) \quad (S6)$$

where $\sigma_M(N(t)) \equiv \sqrt{a + \lambda(N(t)) M(t) + b}$.

Equation (7):
$$\frac{\langle dX(t) \rangle}{dt} = \frac{b}{M(t)+1} (\beta - X(t))$$

By taking a time interval dt so small, we argue situations that at most one cell increases or decreases mutually exclusively in dt . This condition requires decay rate is small especially while the cell number is large; $\lambda(X(t)) M(t) dt \ll 1$ and $(a+b)dt \ll 1$. Therefore, we exclude catastrophic states from the application of this analysis.

In the increase process of cell number that are described by Eqs. (1) and (2), the cell ratio $X(t) \equiv N_I(t)/(N_I(t) + N_{II}(t))$ increases with a probability $(aX(t) + b_I)dt$ by adding one type-I cell. The change of $X(t)$ is:

$$\begin{aligned} dX(t) &= X(t+dt) - X(t) = \frac{N_I(t) + 1}{N_I(t) + N_{II}(t) + 1} - \frac{N_I(t)}{N_I(t) + N_{II}(t)} \\ &= \frac{N_I^2(t) + N_I(t)N_{II}(t) + N_I(t) + N_{II}(t) - (N_I^2(t) + N_I(t)N_{II}(t) + N_I(t))}{(N_I(t) + N_{II}(t) + 1)(N_I(t) + N_{II}(t))} \\ &= \frac{N_{II}(t)}{(N_I(t) + N_{II}(t) + 1)(N_I(t) + N_{II}(t))} \\ &\therefore X(t+dt) - X(t) = \frac{1-X(t)}{M(t)+1} \end{aligned} \quad (S7),$$

where $M(t) \equiv N_I(t) + N_{II}(t)$. In the increase process of cell number, the ratio $X(t)$ decreases with a probability $(a(1-X(t)) + b_{II})dt$ by adding one type-II cell. The change of $X(t)$ is:

$$\begin{aligned}
dX(t) &= X(t+dt) - X(t) = \frac{N_I(t)}{N_I(t) + N_{II}(t) + 1} - \frac{N_I(t)}{N_I(t) + N_{II}(t)} \\
&= \frac{N_I^2(t) + N_I(t)N_{II}(t) - (N_I^2(t) + N_I(t)N_{II}(t) + N_I(t))}{(N_I(t) + N_{II}(t) + 1)(N_I(t) + N_{II}(t))} = \frac{-N_I(t)}{(N_I(t) + N_{II}(t) + 1)(N_I(t) + N_{II}(t))} \\
&\therefore X(t+dt) - X(t) = -\frac{X(t)}{M(t) + 1} \quad (S8).
\end{aligned}$$

Note that we ignore the small probability of two different increase process occurs in the same infinitesimal time interval dt .

In the decay process of cells described in Eq. (3), we argue the composition change under conditions where at most one cell disappears in the same infinitesimal time interval dt with assuming $\lambda(X(t))M(t)dt \ll 1$. Under this condition, through the decay process, $X(t)$ increases with a probability $\lambda(X(t))N_{II}(t)dt = (1 - X(t))\lambda(X(t))M(t)dt$ by removing one type-II cell. The change of $X(t)$ is:

$$\begin{aligned}
dX(t) &= X(t+dt) - X(t) = \frac{N_I(t)}{N_I(t) + N_{II}(t) - 1} - \frac{N_I(t)}{N_I(t) + N_{II}(t)} \\
&= \frac{N_I^2(t) + N_I(t)N_{II}(t) - (N_I^2(t) + N_I(t)N_{II}(t) - N_I(t))}{(N_I(t) + N_{II}(t) - 1)(N_I(t) + N_{II}(t))} \\
&= \frac{N_I(t)}{(N_I(t) + N_{II}(t) - 1)(N_I(t) + N_{II}(t))} \\
&\therefore X(t+dt) - X(t) = \frac{X(t)}{M(t) - 1} \quad (S9).
\end{aligned}$$

Through the decay process, $X(t)$ decreases with a probability $\lambda(X(t))N_I(t)dt = X(t)\lambda(X(t))M(t)dt$ by removing one type-I cell. The change of $X(t)$ is:

$$\begin{aligned}
dX(t) &= X(t+dt) - X(t) = \frac{N_I(t) - 1}{N_I(t) + N_{II}(t) - 1} - \frac{N_I(t)}{N_I(t) + N_{II}(t)} \\
&= \frac{N_I^2(t) + N_I(t)N_{II}(t) - N_I(t) - N_{II}(t) - (N_I^2(t) + N_I(t)N_{II}(t) - N_I(t))}{(N_I(t) + N_{II}(t) - 1)(N_I(t) + N_{II}(t))} \\
&= \frac{-N_{II}(t)}{(N_I(t) + N_{II}(t) - 1)(N_I(t) + N_{II}(t))} \\
&\therefore X(t+dt) - X(t) = -\frac{1 - X(t)}{M(t) - 1} \quad (S10).
\end{aligned}$$

Taken Eqs. (S7-S10) together, we obtain the expectation of the change of $X(t)$ during an infinitesimal time interval $[t, t+dt]$:

$$\begin{aligned}
\langle dX(t) \rangle &= (aX(t) + b_I)dt \frac{1 - X(t)}{M(t) + 1} - (a(1 - X(t)) + b_{II})dt \frac{X(t)}{M(t) + 1} \\
&\quad + \lambda(X(t))M(t)(1 - X(t))dt \frac{X(t)}{M(t) - 1} - \lambda(X(t))M(t)X(t)dt \frac{1 - X(t)}{M(t) - 1} \\
&= \frac{b_I(1 - X(t)) - b_{II}X(t)}{M(t) + 1} dt = \frac{b\beta(1 - X(t)) - b(1 - \beta)X(t)}{M(t) + 1} dt = \frac{b(\beta - X(t))}{M(t) + 1} dt \quad (S11) = (7),
\end{aligned}$$

where $b \equiv b_I + b_{II}$ and $\beta \equiv b_I/b$. This calculation demonstrates that the expected value of $X(t+dt)$ is equal to $X(t)$ in MTA with $b = 0$. This demonstrates that the stochastic processes of proliferation and decay are a martingale, whereas actual biological systems require non-zero b to avoid the extinction of either cell type.

Equations (9-10):
$$\frac{v(dX(t))}{dt} \cong 2a \frac{X(t)(1-X(t))}{M^2(t)} + b \frac{X(t) - 2\beta X(t) + \beta}{M^2(t)}$$

We obtain the variance of $dX(t)$ from Eqs. (S7-S10):

$$\begin{aligned}
V(dX(t)) + \langle dX(t) \rangle^2 &= (aX(t) + b\beta)dt \frac{(1 - X(t))^2}{(M(t) + 1)^2} + (a(1 - X(t)) + b(1 - \beta))dt \frac{X^2(t)}{(M(t) + 1)^2} \\
&\quad + \lambda(X(t))M(t)(1 - X(t))dt \frac{X^2(t)}{(M(t) - 1)^2} + \lambda(X(t))M(t)X(t)dt \frac{(1 - X(t))^2}{(M(t) - 1)^2} \\
&= X(t)(1 - X(t)) \left(\frac{a}{(M(t) + 1)^2} + \frac{\lambda(X(t))M(t)}{(M(t) - 1)^2} \right) dt + \frac{b\beta(1 - X(t))^2 + b(1 - \beta)X^2(t)}{(M(t) + 1)^2} dt \\
&= X(t)(1 - X(t)) \left(\frac{a}{(M(t) + 1)^2} + \frac{\lambda(X(t))M(t)}{(M(t) - 1)^2} \right) dt + \frac{b(X^2(t) - 2\beta X(t) + \beta)}{(M(t) + 1)^2} dt \quad (S12).
\end{aligned}$$

Since $\langle dX(t) \rangle^2$ is much smaller than $V(dX(t))$ due to the factor $(dt)^2$, the variance of $X(t)$ change is described by Eq. (8). Further, when we approximate $M(t) \cong M(t) + 1 \cong M(t) - 1$ and $\lambda(X(t))M(t) \cong a + b$ under conditions $M(t) \gg 1$ and $\lambda(X(t))M(t) \cong a + b$, we simplify:

$$\begin{aligned}
\frac{V(dX(t))}{dt} &\cong \frac{X(t)(1 - X(t)) \left((a + \lambda(X(t))M(t)) + b(X^2(t) - 2\beta X(t) + \beta) \right)}{(M(t))^2} \\
&\cong \frac{X(t)(1 - X(t))(a + a + b) + b(X^2(t) - 2\beta X(t) + \beta)}{M^2(t)} \\
&= \frac{2aX(t)(1 - X(t)) + b(X(t) - 2\beta X(t) + \beta)}{M^2(t)} \quad (S13) = (9).
\end{aligned}$$

Thus, we obtain Eq. (9) and the following Eq. (10):

$$\sigma^2(X(t)) = 2aX(t)(1 - X(t)) + b((1 - \beta)X(t) + \beta(1 - X(t))) \quad (10).$$

Since $X(t)$ is a ratio in range $[0, 1]$, the first term in the right-hand side of Eq. (10) yields a value in range $[0, a/2]$. The second term yields a value in range $[b\beta, b(1 - \beta)]$. Therefore, the minimum value of $\sigma^2(X(t))$ is larger than the smaller of $\{b\beta, b(1 - \beta)\}$ and the maximum value of $\sigma^2(X(t))$ is smaller than $a/2$ + the larger of $\{b\beta, b(1 - \beta)\}$. For example, under the Fig. 1D MTA condition with $a = 0.1$, $b = 0.001$, and $\beta = 0.5$, $\sigma^2(X(t))$ yields the minimum value 0.0005 when $X(t) = 0$ or 1, and the maximum value 0.0505 when $X(t) = 0.5$. Under the Fig. 1J CSC condition with $a = 0$, $b = 0.1$, and $\beta = 0.33$, $\sigma^2(X(t))$ yields the minimum value 0.033 when $X(t) = 0$, and the maximum value 0.066 when $X(t) = 1$. The minimum of $\sigma^2(X(t))$ can be 0, when $X(t) = 0$ or 1 under the condition $b = 0$, indicating the extinction of either cell type. Even under the condition of $b \cong 0$, if $X(t) \neq 0$ and $X(t) \neq 1$, $\sigma^2(X(t)) \neq 0$. Therefore, when we set $0 < a + b \ll 1$ using a sufficiently small time-unit and $X(t)$ is far from the boundary, the variance of $dX(t)$ is largely depending on $M(t)$. Taken together, under conditions $\lambda(X(t))M(t) \cong a + b$, $M(t) \gg 1$, $N_I(t) = M(t)X(t) \gg 1$, and $N_{II}(t) = M(t)(1 - X(t)) \gg 1$, we approximate $V(dX(t))/dt \cong \sigma^2/M(t)$ using a constant parameter σ . These conditions indicate that both cell types exist in sufficiently large numbers under non-catastrophic states. Particularly, when $X(t) \cong \alpha$, which requires MTA condition $a \gg b$ or CSC condition $\beta \cong \alpha$, substituting to Eq. (10) gives Eq. (12): $\sigma^2 = 2a\alpha(1 - \alpha) + b(\alpha + \beta - 2a\beta)$. When $X(t) \cong \beta$ in the CSC regime, substituting to Eq. (10) gives: $\sigma^2 = 2a\beta(1 - \beta) + b((1 - \beta)\beta + \beta(1 - \beta)) = 2(a + b)\beta(1 - \beta)$.

Equation (20): $dY_t = kY_t^2 dW_t$

To solve Eq. (20) SDE, we use Itô's formula. For a general SDE of the form:

$$dX_t = \mu_t dt + \sigma_t dW_t \quad (S14),$$

where W_t is a Wiener process, Itô's formula gives:

$$df(t, x) = \left(\frac{\partial f}{\partial t} + \mu_t \frac{\partial f}{\partial x} + \frac{\sigma_t^2}{2} \frac{\partial^2 f}{\partial x^2} \right) dt + \sigma_t \frac{\partial f}{\partial x} dW_t \quad (S15).$$

In the case of Eq. (20), we set $\mu_t = 0$ and $\sigma_t = kY_t^2$. Let us consider the transformation:

$$Z_t = \frac{1}{kY_t} \quad (S16).$$

Then the derivatives are:

$$\frac{\partial Z_t}{\partial y} = -\frac{1}{k Y_t^2}, \frac{\partial^2 Z_t}{\partial y^2} = \frac{2}{k Y_t^3}, \frac{\partial Z_t}{\partial t} = 0 \quad (\text{S17}).$$

Substituting into Itô's formula Eq. (S15), we obtain Eq. (21):

$$\begin{aligned} dZ_t &= \left(\frac{\partial Z_t}{\partial t} + 0 \frac{\partial Z_t}{\partial y} + \frac{k^2 Y_t^4}{2} \frac{\partial^2 Z_t}{\partial y^2} \right) dt + k Y_t^2 \frac{\partial Z_t}{\partial y} dW_t = \frac{k^2 Y_t^4}{2} \frac{2}{k Y_t^3} dt - k Y_t^2 \frac{1}{k Y_t^2} dW_t \\ &= k Y_t dt - dW_t \\ \therefore dZ_t &= \frac{1}{Z_t} dt - dW_t \quad (\text{S18}) = (21). \end{aligned}$$

Equation (22):

$$p(y, t|Y_0) = \frac{Y_0}{\sigma k \sqrt{2\pi t} y^3} \left(\exp\left(-\frac{1}{2\sigma^2 k^2 t} \left(\frac{1}{y} - \frac{1}{Y_0}\right)^2\right) - \exp\left(-\frac{1}{2\sigma^2 k^2 t} \left(\frac{1}{y} + \frac{1}{Y_0}\right)^2\right) \right)$$

To solve Eq. (20), we refer to the solution of the SED (Eq. S18), which is known as the three-dimensional Bessel process (23). The probability density distribution of Z_t that follows Eq. (S18) is:

$$\begin{aligned} p_Z(z, t|Z_0) &= \frac{1}{t} \frac{z\sqrt{z}}{\sqrt{Z_0}} \exp\left(-\frac{z^2 + Z_0^2}{2t}\right) \left(\frac{\exp\left(\frac{Z_0 z}{t}\right) - \exp\left(-\frac{Z_0 z}{t}\right)}{\sqrt{2\pi \frac{Z_0 z}{t}}} \right) \\ &= \frac{z}{Z_0 \sqrt{2\pi t}} \left(\exp\left(-\frac{(z-Z_0)^2}{2t}\right) - \exp\left(-\frac{(z+Z_0)^2}{2t}\right) \right) \quad (\text{S19}), \end{aligned}$$

where Z_0 denotes the initial value. To obtain the probability density distribution of $Y_t = |X(t/\sigma^2) - \alpha|$ after t repetitions of proliferation and decay in the stochastic simulation of two cell populations, we replace t with $\sigma^2 t$, and apply the change of variable $z = 1/(ky)$. Then, we obtain probability density function Eq.(22):

$$\begin{aligned} p_Y(y, t|Y_0) &= p_Z\left(\frac{1}{ky}, \sigma^2 t \middle| \frac{1}{kY_0}\right) \cdot \left| \frac{dz}{dy} \right| = p_Z\left(\frac{1}{ky}, \sigma^2 t \middle| \frac{1}{kY_0}\right) \cdot \frac{1}{ky^2} \\ &= \frac{\frac{1}{ky}}{k y^2 \sqrt{2\pi \sigma^2 t} \frac{1}{kY_0}} \left(\exp\left(-\frac{\left(\frac{1}{ky} - \frac{1}{kY_0}\right)^2}{2\sigma^2 t}\right) - \exp\left(-\frac{\left(\frac{1}{ky} + \frac{1}{kY_0}\right)^2}{2\sigma^2 t}\right) \right) \\ \therefore p_Y(y, t|Y_0) &= \frac{Y_0}{k \sigma \sqrt{2\pi t} y^3} \left(\exp\left(-\frac{1}{2\sigma^2 t k^2} \left(\frac{1}{y} - \frac{1}{Y_0}\right)^2\right) - \exp\left(-\frac{1}{2\sigma^2 t k^2} \left(\frac{1}{y} + \frac{1}{Y_0}\right)^2\right) \right) \quad (\text{S20}). \end{aligned}$$